


The Complex-Pole Filter Representation (COFRE) for spectral modeling of fNIRS signals

Marco A. Pinto Orellana ^{a,*}, Peyman Mirtaheeri ^a, Hugo L. Hammer ^{b,c}

^a*Department of Mechanical, Electronics and Chemical Engineering. Oslo Metropolitan University.*

^b*Department of Information Technology. Oslo Metropolitan University.*

^c*Department of Holistic Systems, Simula Metropolitan Center for Digital Engineering.*

Abstract

The complex-pole frequency representation (COFRE) is introduced in this paper as a new approach for spectrum modeling in biomedical signals. Our method allows us to estimate the spectral power density at precise frequencies using an array of narrow band-pass filters with single complex poles. Closed-form expressions for the frequency resolution and transient time response of the proposed filters have also been formulated. In addition, COFRE filters have a constant time and space complexity allowing their use in real-time environments. Our model was applied to identify frequency markers that characterize tinnitus in very-low-frequency oscillations within functional near-infrared spectroscopy (fNIRS) signals. We examined data from six patients with subjective tinnitus and seven healthy participants as a control group. A significant decrease in the spectrum power was observed in tinnitus patients in the left temporal lobe. In particular, we identified several tinnitus signatures in the spectral hemodynamic information, including (a.) a significant spectrum difference in one specific harmonic in the metabolic/endothelial frequency region, at 7mHz, for both chromophores and hemispheres; and (b.) a significant differences in the range 30-50mHz in the neurogenic/myogenic band.

Keywords: Tinnitus, Spectral representation, Filter bank, Infinite impulse response filter, Functional near-infrared spectroscopy.

1. Introduction

Tinnitus is an unintentional experience of meaningless sounds in the absence of external sources [1, p. 230; 2, p. 121] and it can be primarily affected by environmental and physiological factors [3–5]. This type of auditory hallucination provokes neural oscillation patterns in the auditory cortex that resemble waveforms generated due to sound stimuli [2, p. 121-122]. We contribute to analyzing this health condition by providing a method for extracting accurate hemodynamic information in the spectrum domain.

Tinnitus involves a rise in spontaneous firing and synchronization of the neuronal activity in the auditory cortex. These changes induce variations in the spectral properties of the patient's brain hemodynamic and electrical signals. For instance, changes in the spectrum power in brain signals play an essential function in predicting of a chronic tinnitus level [1, p. 163]. In addition, tinnitus-provoked increments of the synaptic metabolism lead to abnormal transient responses in the oxy-hemoglobin concentration [6, p. 57]. Furthermore, drastic syncope-inducing shifts

*Corresponding author

of low blood pressure on the brain, which involve sudden hemodynamic imbalances, can also generate episodes of tinnitus [1, p. 88].

These tinnitus-associated hemodynamic changes have often been studied using functional near-infrared spectroscopy (fNIRS) as an imaging method. fNIRS is a non-invasive imaging technique for measuring concentration changes of chromophores, oxy-hemoglobin (HbO) and deoxy-hemoglobin (HbR), using light in the near-infrared region (700-900 nm). In a conventional continuous fNIRS device, two light sources separated by 2–3 cm with different optical wavelengths emit light to the brain. Chromophore concentrations are then estimated from the received light intensity using the modified Beer-Lambert law. Research from Sevy et al. [7] and Olds et al. [8] validated fNIRS to detect tinnitus-cause hemodynamic variations during cortical stimulation in patients with severe auditory deficits with cochlear implants. Later experiments used fNIRS to illustrate that tinnitus patients exhibit certain unique phenomena in the temporal region due to their anatomical closeness to the auditory cortex: (a.) higher HbO concentrations in the left hemisphere compared with a healthy-subject baseline [9]; (b.) general activation in both hemispheres [9]; and (c.) activation steadiness even during quiet periods while activation reduction is visible in healthy subjects [10].

Blood flow biosignals generally describe the characteristics of certain physiological signals according to their spectrum properties in five main frequency bands: endothelial/metabolic (3-20mHz), neurogenic (20-50mHz), myogenic (50-150mHz), respiratory (0.15-0.4Hz) or cardiac (0.4-2.0Hz) [11–13]. In this paper, we denoted this frequency classification as the ENMRC (endothelial-neurogenic-myogenic-respiratory-cardiac) scale. The frequency association of this spectral division with vasomotion and neural activity was first investigated by Kastrup et al. [14] and later verified by Soderstrom et al. [15]. ENMRC has also been successfully extrapolated to fNIRS for monitoring patients in an intensive care unit [16] in order to recognize variations in connectivity and muscle exhaustion [17], cognitive activities [18], physical activity [19] or sleep [20].

The ability to distinguish spectral-specific responses is a primary advantage of the ENMRC frequency division. For instance, the endothelial band denotes the highest wavelet coherence during arithmetic-based tasks [18]. Besides, exercise performance efficiency positively correlates with spectrum power in the neurogenic band while negatively correlated in the endothelial band [20].

The metabolic, neurogenic and myogenic intervals of the ENMRC frequency division fall within the category of very-low-frequencies [14]. Estimating the power spectrum density at these frequency intervals is a challenge given that a long sample period is required (an endothelial wave could need up to 333.3 seconds to complete a single cycle). Besides, each spectrum estimation approach may lead to different outcomes with contrasting bias and variances [21]. Furthermore, spectrum estimators such as Welch or autoregressive-based methods cannot provide reliable values for narrow frequencies. Due to these conditions, an alternative approach for defining the spectrum power at localized frequencies is to use an array (or bank) of narrow bandpass, anti-notch filters. Each of the filters in this set can be calibrated to define only one desired frequency with a certain tolerance. To the best of our knowledge, only Folgosi-Correa and Nogueira suggested a method with a similar aim [22]. However, the latter limited their analysis to broader frequency bands (higher than 45mHz) with traditional Butterworth frequency filters without further mathematical treatment.

Based on the filter-bank spectral representation of a stationary signal, we propose a new spectrum estimation approach that relies on first-order, complex, infinite impulse response filters: the complex-pole filter representation (COFRE). We developed several properties from

COFRE filters that allow us to configure their frequency resolution (and optimizing frequency peak identification) or enhance their time response (for real-time applications). Our method is used to accurately discover discriminatory frequency signatures on fNIRS signals between patients with tinnitus and healthy control groups. The tinnitus spectral signatures are then interpreted within the ENMRC spectral division that serves us as a biological interpretation framework for the detected spectral differences. In the following sections, we introduce the formal definition of the alternative filter bank representation, the COFRE method and the properties of its filters, and the results of its application on the tinnitus dataset.

2. COFRE: Complex-pole filter representation

2.1. Filter-bank spectral representation

Most biomedical signals have non-stationary characteristics, i.e., their statistical properties can change over time. Khoa et al. suggested using Wavelets to model non-stationary signals affected by trends, drifts, or event-based changes [23]. However, under normal circumstances, physiological signals can be successfully approximated as local-stationary in short time intervals [24, p. 390; 25].

Let us assume, therefore, that an fNIRS signal can be modeled by a wide-sense stationary process (WSS) in a sufficiently small time interval $t \in [t_0, t_1]$ with local stationarity properties [25]. WSS processes denote a finite and time-invariant first and second statistical moment, with a power spectrum density defined as the Fourier transform of its autocorrelation function $\gamma_{xx}(\tau) = \mathbb{E}[X^*(t)X(t+\tau)]$ [21, p. 57]:

$$S_x(\omega) = \int_{-\infty}^{\infty} \gamma_{xx}(\tau) e^{-j2\pi\omega\tau} d\tau \quad (1)$$

Consequently, given an observed time series $\{x(t)|t = 1, 2, \dots, T\}$ of the process $X(t)$, we can define the estimator of the autocorrelation as

$$\hat{\gamma}_{xx}(\tau) = \frac{1}{T} \sum_{t=1}^{T-1-\tau} x^*(t) x(t+\tau) = \frac{1}{T} x^*(-\tau) * x(\tau) \quad (2)$$

where $*$ represents the convolution operation, and x^* is the complex conjugate of x .

Then, the estimator $\hat{\gamma}_{xx}(\tau)$ can be used to obtain an estimation of the spectrum,

$$\hat{S}_x(\omega) = \sum_{\tau=0}^T \hat{\gamma}_{xx}(\tau) e^{-j2\pi\tau\frac{\omega}{f_s}} \quad (3)$$

where ω is the normalized frequency with respect to the sampling frequency f_s : $\omega = \frac{f}{f_s}$, $\omega \in [0, 1/2]$.

Recall that the spectrum can be non-parametrically expressed through the discrete Fourier transform (DFT) of the realization $x(t)$:

$$\hat{S}_x(\omega) = \frac{1}{T} \sum_{\tau=0}^T x^*(-\tau) * x(\tau) e^{-j2\pi\tau\frac{\omega}{f_s}} = \frac{1}{T} |X(e^{j2\pi\omega})|^2 \quad (4)$$

where $X(e^{j2\pi\omega})$ is the DFT of $x(t)$. Convergence properties of a tapped-version of Equation 4 are discussed in [26, pp.255-257, Theorem 7.1].

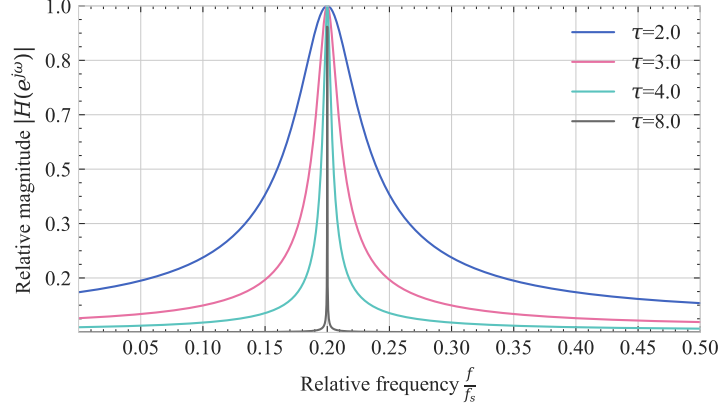


Figure 1: Magnitude response $|H(e^{j\omega})|$ of a complex narrow-band pass filter when $\omega^* = 0.2$.

We should denote that due to the constraints inherited from $X(e^{j2\pi\omega})$, $\hat{S}_X(\omega)$ has a frequency resolution ($\omega \in [0, 1/2]$):

$$\Delta_{FFT}\omega = \frac{1}{T} \quad (5)$$

Now, let us define a filtering process $m_\omega(t)$ which spectrum can be described by

$$M_w(\omega) = \begin{cases} 1 & \omega = \omega^* \\ 0 & |\omega - \omega^*| \geq \Delta_{FFT}\omega \end{cases} \quad (6)$$

with the further restriction that $M_\omega(\omega) \leq \varepsilon < 1$ where $0 < |\omega - \omega^*| \leq \Delta_{FFT}\omega$.

Therefore, DFT can be expressed as a sum of a family of narrow-band pass filters $\{M_{k\Delta_{FFT}\omega}(\omega) \mid k = 0, 1, \dots, \lfloor \frac{T}{2} \rfloor\}$:

$$X^f(e^{j2\pi\omega}) = \sum_{k=0}^{\lfloor \frac{T}{2} \rfloor} M_{k\Delta_{FFT}\omega}(\omega) X(e^{j2\pi\omega}) \quad \omega \in W = \left\{0, \Delta_{FFT}\omega, \dots, \left[\frac{T}{2}\right]\Delta_{FFT}\omega\right\} \quad (7)$$

Note that $M_\omega(\omega)$ can also be interpreted as a spectrum smoothing function in the interval $\omega^* - \Delta_{FFT}\omega < \omega < \omega^* + \Delta_{FFT}\omega$.

Finally, the spectrum in the entire support W can also be expressed as a filter sum:

$$\hat{S}_x(\omega) = \frac{1}{T} \left| X^f(e^{j2\pi\omega}) \right|^2 \quad \omega \in W \quad (8)$$

Alternatively, the spectrum at a specific frequency ω_0 can be estimated using a filter M_{ω_0} :

$$\hat{S}_x(\omega = \omega_0) = \frac{1}{T} |M_{\omega_0}(\omega)|^2 \left| X(e^{j2\pi\omega_0}) \right|^2 \quad (9)$$

2.2. Complex-pole narrow bandpass filter

The COFRE spectral representation relies in the use of an array of narrow-bandpass filters. These filters \mathcal{H}_k are infinite impulse response (IIR) filters with a single complex pole by construction.

Given a real-valued input signal $x(t)$, let us define a complex-output filter \mathcal{H} that maps $x \mapsto y$:

$$y(t) = \phi y(t-1) + x(t) \quad (10)$$

where $y(t)$ is the complex-valued filtered signal, and ϕ is the complex autoregressive coefficient: $\phi = \rho e^{j\omega^*}$.

Using the a lag operation L defined as $L^\ell x(t) = x(t - \ell)$, we can formulate \mathcal{H} as:

$$\mathcal{H}x(t) = (1 - \phi L^1)^{-1} x(t) \quad (11)$$

The intrinsic frequency properties of \mathcal{H} can be described through its transfer function (TF) in the z -domain. TF can be naturally extracted by inverting Equation 11 after replacing $L = z^{-1}$:

$$H(z) = \frac{1}{1 - \rho e^{j2\pi\omega^*} z^{-1}} = F(z; \rho, \omega^*) \quad (12)$$

In consequence, the filter magnitude response, or gain function, $M(\cdot)$ depends on the system frequency and it is described by

$$M(\omega; \rho, \omega^*) = \left| H(e^{j2\pi\omega}) \right| = \frac{1}{|1 - \rho e^{j2\pi(\omega^* - \omega)}|} \quad (13)$$

where the ω is the normalized signal frequency: $\omega = \frac{f}{f_s}$, f is the signal frequency in Hz, and f_s is the sampling rate of the signal.

The complex autoregressive coefficient ϕ reflects some significant characteristics of the filter magnitude response: the filter has a **symmetric** response around ω^* where the filter also denotes its maximum gain (Figure 1.A). These properties are formalized in Lemma 1 and Lemma 2.

Lemma 1 (Symmetry response). *A complex single-pole IIR filter defined by the transfer function $M(\omega; \rho, \omega^*)$ is symmetric around ω^* , i.e., $M(\omega; \rho, \omega^* - \Delta\omega) = M(\omega; \rho, \omega^* + \Delta\omega)$ $\Delta\omega \in [0, \frac{1}{2}]$.*

Proof. Proof in Section A.1. □

Lemma 2 (Unique maximum). *The filter $M(\omega; \rho, \Delta\omega)$ has a single and unique maximum located at ω^* and*

$$\max M(\omega; \rho, \omega) = M(\omega; \rho, \omega^*) = |1 - \rho|^{-1} \quad (14)$$

Proof. Proof in Section A.2. □

Let us now reparametrize the coefficient modulus ρ (Equation 13) by introducing a new variable: the *frequency bandwidth* τ such that $\rho = 1 - e^{-\tau}$. Filters with lower values of τ have a wide symmetric response around ω^* . In comparison, higher τ values will induce very narrow filters (Figure 1.A). To ensure the filter is stationary (and therefore, stable), the condition $|\phi| < 1$ should be satisfied, or equivalently, $|\rho| < 1$ or $\tau > 0$.

Furthermore, as a direct consequence of Equation 10 and Equation 13, it is remarkable that the filter $F(z; \rho, \omega^*)$ will be conditioned by two main constraints: its maximum frequency resolution and its transient response. For the purpose of this paper, we formalized these concepts with the following definitions:

Definition 3 (Frequency resolution). *Given a cut-off factor $\alpha \in (0, 1)$, define the frequency resolution $\Delta\omega > 0$ as the frequency distance that satisfies*

$$M(\omega; \rho, \omega) \geq \alpha M(\omega; \rho, \omega^*) \quad \forall \omega \in [\max(0, \omega^* - \Delta\omega), \min(\pi, \omega^* + \Delta\omega)] \quad (15)$$

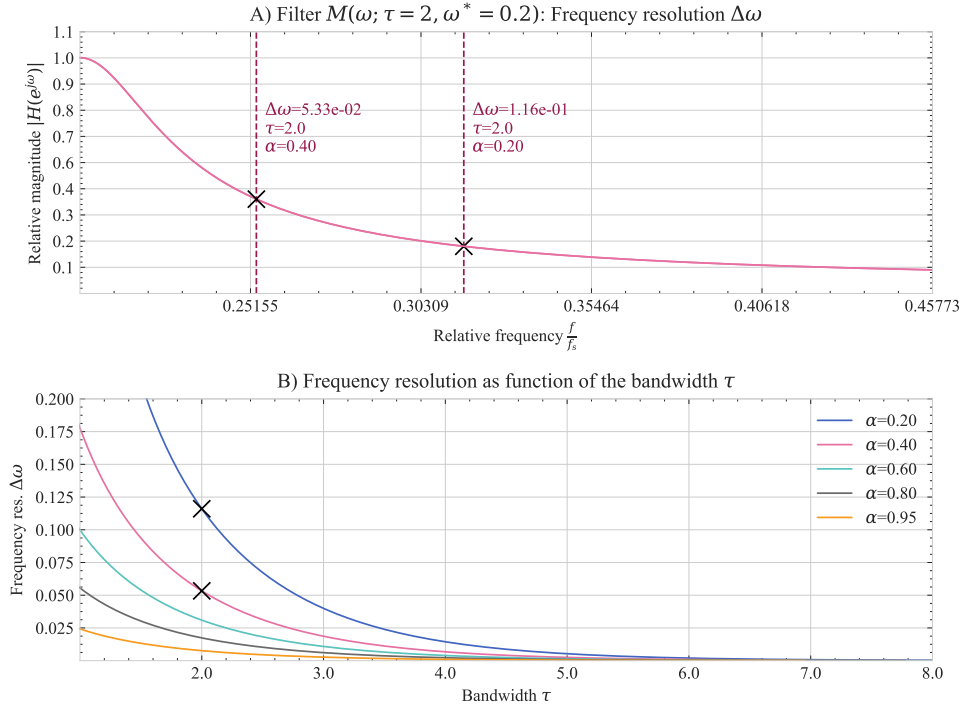


Figure 2: Frequency resolution of a complex narrow-band pass filter: A) Visual interpretation of two frequency resolutions with respect to the filter magnitude response (Definition 3). B) Curves of the frequency resolution with respect to the bandwidth τ and cut-offs α (Lemma 6).

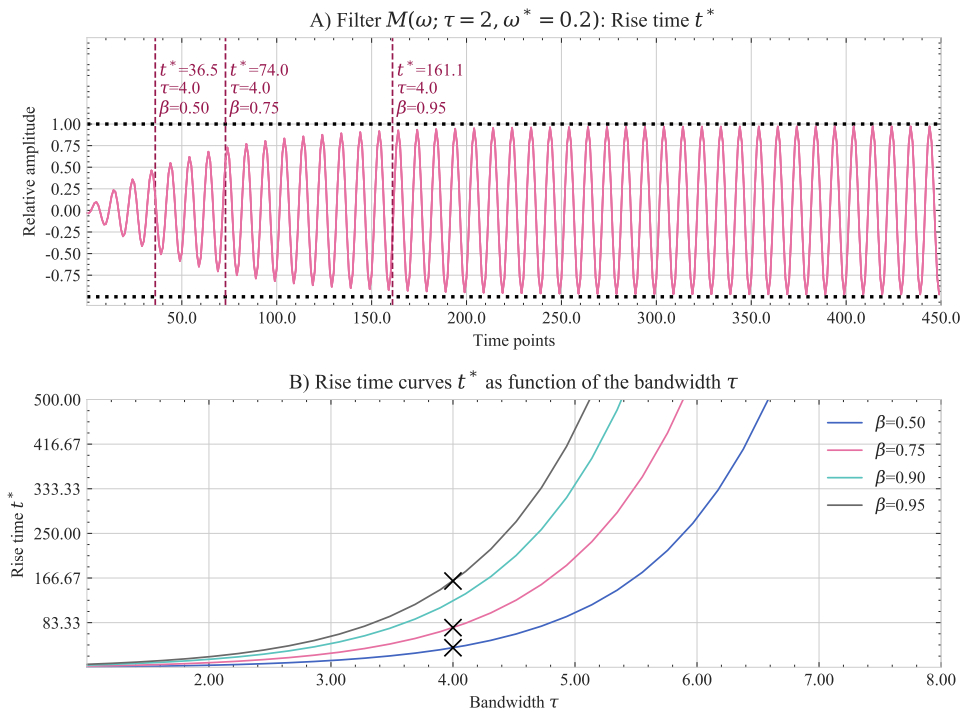


Figure 3: Rise-time (transient time response) of a complex narrow-band pass filter: A) Visual interpretation of three rise-time parameters with respect to the transient response of $\Re\{y(t)\}$ with a sinusoid input signal (Definition 5). B) Curves of the rise time with respect to the bandwidth τ and cut-offs β (Lemma 8).

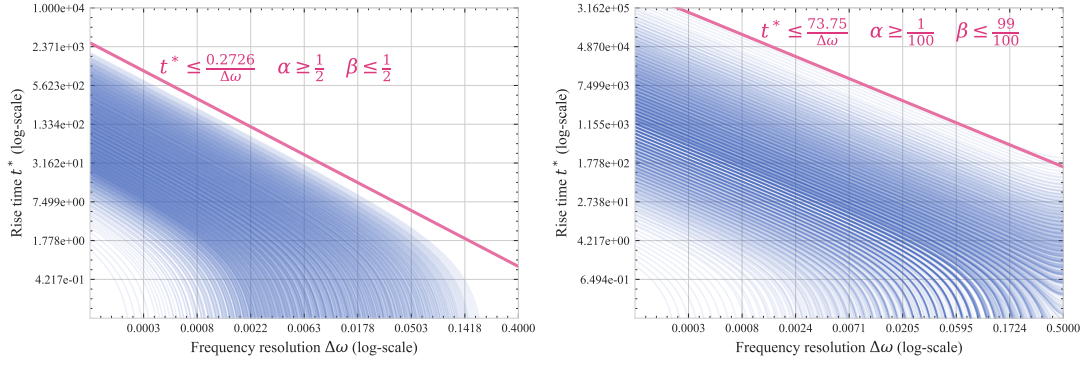


Figure 4: Joint time-frequency $(t^*, \Delta\omega)$ curves for several cut-off intervals of α and β along with their respective upper-bounds described in Lemma 10.

Corollary 4. *Due to the convexity of $M(\omega; \rho, \omega)$, the frequency resolution $\Delta\omega$ also satisfies*

$$M(\omega; \rho, \omega^* \pm \Delta\omega) = \alpha M(\omega; \rho, \omega^*) \quad (16)$$

Definition 5 (Rise or transient time). *Given a cut-off $\beta \in (0, 1)$ and an input signal $x(t) = \cos(\omega^*t)$, define the rise time t^* as the time point such that*

$$\mathcal{Re}\{y(t)\} \geq \beta x(t) \quad \forall t \geq t^* \quad (17)$$

The interpretation of t^* and $\Delta\omega$ is straightforward: the frequency resolution $\Delta\omega$ sets the frequency radius where the filter has a proportion α of its peak response (Figure 2). On the time-domain, the rise time t^* estimates the number of points that the filter requires to start providing a steady-state output (Figure 3). Both constraints have closed-form expressions that depend only on the filter bandwidth τ and central frequency ω^* as the following lemmas and corollaries denote.

Lemma 6 (Frequency resolution configuration). *The cosine of the frequency resolution of a filter $M(\omega; \rho, \omega^*)$ is a second-order rational function of the complex autoregressive modulus ρ :*

$$\Delta\omega = \frac{1}{2\pi} \arccos\left(\frac{1}{2\rho} (\rho^2 + 1 - \alpha^{-2} (1 - \rho)^2)\right) \quad (18)$$

Proof. Proof in Section A.3. □

Corollary 7 (Frequency-optimal bandwidth). *The minimum bandwidth τ to ensure a frequency resolution $\Delta\omega$ under a cut-off α is given by*

$$\tau = -\log\left(1 - \frac{\cos 2\pi\Delta\omega - \alpha^{-2}}{1 - \alpha^{-2}} - \frac{1}{1 - \alpha^{-2}} \sqrt{\cos^2 2\pi\Delta\omega - (1 - \alpha^{-2})^2}\right) \quad (19)$$

Proof. Proof in Section A.4. □

Lemma 8 (Rise time configuration). *The rise time of a filter $M(\omega; \rho, \omega^*)$ is inversely proportional to the logarithm of ρ and proportional to the logarithm of the complement of the cut-off factor β :*

$$t^* = \log_\rho\left(\frac{1 - \beta}{\rho}\right) = \frac{\log(1 - \beta)}{\log(\rho)} - 1 \quad (20)$$

Proof. Proof in Section A.5. □

Corollary 9 (Time-optimal bandwidth). *The minimum bandwidth τ to ensure a rise time t^* (under a cut-off β) is*

$$\tau = -\log\left(1 - (1 - \beta)^{\frac{1}{1+t^*}}\right) \quad (21)$$

Proof. Proof in Section A.6. □

Lemma 10 (Joint time-frequency constraint). *Given the cut-offs α and β , the rise time t^* and the frequency resolution $\Delta\omega$ are mutually constrained by*

$$t^* \Delta\omega < -\log(1 - \beta) \left(\frac{\sqrt{(\alpha\pi\Delta\omega)^2 - \alpha^2 + 1}}{2\pi\alpha} + \frac{\Delta\omega}{2} \right) \quad (22)$$

Proof. Proof in Section A.7. □

Corollary 11 (Time-frequency uncertainty). *A narrow bandpass filter with a frequency resolution $\Delta\omega < \frac{1}{5}$ has its joint time-frequency resolution upper-bounded by*

$$t^* \Delta\omega < -\log(1 - \beta) \left(\frac{\sqrt{1 - \left(1 - \frac{4}{25}\pi^2\right)\alpha^2}}{2\pi\alpha} + \frac{1}{10} \right) \quad (23)$$

Proof. Proof in Section A.7. □

A graphical representation of the boundaries described in Lemma 10 is shown in Figure 4.

2.3. COFRE spectrum representation

From Equation 7, it is established that the spectrum of a real-valued input signal $x(t)$ can be expressed as the sum of narrow bandpass filters with frequency resolution $D = \Delta_{FFT}\omega$ (Equation 5). We use this property to define an array of single-pole filters $\{F_k(\omega), k = 1, 2, \dots, \lfloor \frac{T}{2} \rfloor\}$ such that

$$F_k(\omega) = F(\omega; \rho = 1 - e^{-\tau}, \omega^* = kD) \quad (24)$$

where the bandwidth τ is adjusted to the aimed frequency resolution (Corollary 7).

Furthermore, it is acknowledged (Equation 9) that the spectrum at a particular frequency $\omega_0 = k_0D$ can be estimated through a unitary gain filter with a central frequency in ω_0 :

$$\hat{S}_x(\omega = k_0D) = \frac{1}{T} \left| \frac{1}{1 - \rho} F_{k_0}(\omega) X(e^{j2\pi k_0D}) \right|^2 \quad (25)$$

where $\frac{1}{1 - \rho} F_{k_0}(\omega)$ has a unit gain at ω_0 : $\left| \frac{1}{1 - \rho} F_{k_0}(\omega_0) \right| = \frac{1}{1 - \rho} |1 - \rho| = 1$.

Note that the inverse Fourier transform of $Y(\omega) = F_{k_0}(\omega) X(e^{j2\pi k_0D})$ is given by Equation 10:

$$y_{k_0}(t) = \mathcal{H}^{k_0D} x(t) = \rho e^{-jk_0D} y_{k_0}(t - 1) + x(t) \quad (26)$$

Recall the Parseval's identity, $\sum_{t=1}^T |x(t)|^2 = \int_{-\pi}^{\pi} |X(e^{j2\pi\omega})|^2 d\omega$, then

$$\sum_{t=1}^T |y(t)|^2 = \int_{-\pi}^{\pi} |Y(e^{j2\pi\omega})|^2 d\omega \approx |Y(e^{j2\pi k_0D})|^2 \quad (27)$$

Alternatively, Equation 25 can be rewritten as

$$\hat{S}_x(\omega = k_0D) = \frac{1}{(1-\rho)^2} \frac{1}{T} \left| Y(e^{j2\pi k_0D}) \right|^2 \approx \frac{1}{(1-\rho)^2} \frac{1}{T} \sum_{t=1}^T |y(t)|^2 \quad (28)$$

Then, we can formulate a spectrum estimator at a frequency $\omega^* = kD$ using the biased variance estimator of the filtered signal at the same frequency, for a sufficiently narrow bandwidth $\tau = -\log(1-\rho)$:

$$\hat{S}_x(\omega^*) = \frac{1}{e^{-2\tau}} \text{var}(\mathcal{H}^{kD}x(t)) \quad (29)$$

2.4. Recursive COFRE estimation

Let us remark $\hat{S}_x^{(T)}(\omega = k_0D)$ as the spectrum estimator obtain from T points (Equation 28):

$$\hat{S}_x^{(T)}(\omega = k_0D) = \frac{1}{e^{-2\tau}} \frac{1}{T} \sum_{t=1}^T |y(t)|^2 \quad (30)$$

Therefore, it is straightforward to estimate the spectrum using $t-1$ points recursively:

$$\hat{S}_x^{(t)}(\omega = k_0D) = \frac{t-1}{t} \hat{S}_x^{(t-1)}(\omega) + \frac{1}{t e^{-2\tau}} |\mathcal{H}^{k_0D}x(t)|^2 \quad (31)$$

Remark that through the autoregressive formulation in Equation 10, $y(t)$ only depends on the previous filtered point $y(t-1)$ and the current new point $x(t)$:

$$\mathcal{H}^{k_0D}x(t) = \rho e^{-jk_0D} \mathcal{H}^{k_0D}x(t-1) + x(t) \quad (32)$$

We should emphasize that this recursive formulation allows a proper estimation of the spectrum for any observation $x(t)$ collected after the rise time $t > t^*$ (Definition 5).

Furthermore, it is evident that this recursive estimation has space and time complexity $O(1)$.

3. Real fNIRS data

In this paper, we use the data provided in [27]. This dataset was collected at the University of Michigan to analyze brain connectivity changes through fNIRS signals, between patients with tinnitus (PT) and a healthy control (HC) group. The study comprised 20Hz-sampled signals in the frontotemporal cortex during the exposition of PT and HC groups to auditory stimuli. Participants included eight recruited healthy subjects (62% males) with an average age of 25.4 years, as well as ten adults with subjective bilateral tinnitus with an average age of 48.7 years (60% males). HC and PT subjects performed three auditory tests to ensure similar physiological conditions: speech reception threshold tests, audiogram exams, and word recognition score tests, that shows no significant difference between the groups discarding a possible objective tinnitus in the PT group.

The experimental procedure consisted of introducing the participants to alternating blocks of silence and sound lasting 18 seconds each period. Auditory stimuli (27 blocks) were evenly divided (and randomly distributed) between three types of stimulus: (a.) single-frequency 700Hz-wave, (b.) single-frequency 8KHz-wave, and (c.) broadband noise. The dataset was recorded using two light sources with wavelengths at 690 nm and 830 nm at a sampling frequency of 20 Hz. For further description of the experimental protocol, we refer to [27].

We use this dataset to identify variations in the overall spectrum between PT and HC groups. For our analysis, we focus on the electrodes T3 and T4 located in the left and right side of the temporal lobe (auditory cortex). Optical intensities from these locations were converted into chromophore concentration changes using the modified Beer-Lambert law:

$$\begin{pmatrix} x_{HbR} \\ x_{HbO} \end{pmatrix} = \frac{1}{L} \left(\begin{pmatrix} \text{DPF}_{\lambda_{690}} & 0 \\ 0 & \text{DPF}_{\lambda_{830}} \end{pmatrix} \begin{pmatrix} \varepsilon_{690,HbR} & \varepsilon_{690,HbO} \\ \varepsilon_{830,HbR} & \varepsilon_{830,HbO} \end{pmatrix} \right)^{-1} \begin{pmatrix} \Delta\mu_{\lambda_{690}} \\ \Delta\mu_{\lambda_{830}} \end{pmatrix} \quad (33)$$

where $\Delta\mu_{\lambda}$ are the changes in absorption in a wavelength λ [28, p. 8], x_c are the estimates of the concentration changes of a chromophore c , $\varepsilon_{\lambda,c}$ are the molar extinction coefficients, DPF_{λ} are the differential pathlength factor for the two wavelengths, and \circ is the Hadamard product operator. For this study, we use $\varepsilon_{690,HbR} = 2051.96$, $\varepsilon_{830,HbR} = 693.4$, $\varepsilon_{690,HbO} = 276.0$, $\varepsilon_{830,HbO} = 974.0$ as defined in [29, 30]. Moreover, we set $\text{DPF}_{\lambda_{690}} = 6.51$ and $\text{DPF}_{\lambda_{830}} = 5.86$ as recommended by [31] for groups with a similar age than the participants in our dataset.

For conciseness in the analysis, let us define the sound spectral contrast $c(\omega)$. This metric is defined as the difference (for a group $g = \{HC, PT\}$) of the estimated spectrum during a sound stimulus and the spectrum estimated during the followed silence period:

$$c(\omega|g) = |S_x(\omega|\text{sound}, g) - S_x(\omega|\text{silence}, g)| \quad (34)$$

We assume that $S_x(\omega|\text{sound}, g)$ and $S_x(\omega|\text{silence}, g)$ are uncorrelated. Therefore, $c^2(\omega_i|g) \perp c^2(\omega_j|g) \forall i \neq j$,

Now, let us define the inter-group contrast $d(\omega)$ as the difference between the sound spectral contrast in the TP and HC:

$$d(\omega) = c(\omega|\text{TP}) - c(\omega|\text{HC}) \quad (35)$$

Due to the uncorrelatedness property of $c(\omega|g)$, and the central limit theorem, it is known that the limiting distribution of the estimator for the expected value $\mathbb{E}[d(\omega)] = \bar{d}(\omega)$ follows a normal distribution:

$$\bar{d}(\omega) \sim \mathcal{N}(d_0(\omega), \sigma_d^2(\omega)) \quad (36)$$

4. Results and discussion

We analyzed the inter-group contrast $d(\omega)$ for oxy- and deoxy-hemoglobin in patients with tinnitus (PT) and a healthy control (HC) group at several frequencies in the ENMRC scale [11–13]. For this procedure, data from seven subjects (Z04, Z05, Z16, and Z23 in HC, and Z07, Z09, and Z20 in the PT group) were omitted due to quality issues. We estimated the spectrum in 93 specific harmonics distributed on the overall spectrum of interest (3mHz-2Hz). Each one of the five components in the ENMRC scale was divided into segments with uniform separations of 1mHz (endothelial), 1.2mHz (neurogenic), 5mHz (myogenic), 25mHz (respiratory), 70mHz (cardiac). This division ensures that each oscillation category was split into 12-22 segments.

Remark that based on the [Corollary 11](#), we can expect that the rise time (time transient response) will be lower than 272.6 seconds for a minimum frequency resolution of 1mHz (using the cut-offs $\alpha = \beta = \frac{1}{2}$) at a sampling frequency of $f_s = 20\text{Hz}$. Fast Fourier transform (FFT) requires at least $N = \frac{f_s}{\Delta\omega} = \frac{20}{0.0005} = 4e5$ data points, or $2e4$ seconds, to provide a similar frequency resolution. For our analysis, we decided to configure COFRE filters with bandwidths $\tau = 8.65$ such that the frequency resolution is $\Delta\omega = 0.9656\text{mHz}$ ($\alpha = \frac{3}{4}$) with a rise time $t^* = 3956.62 = 42.8212\text{s}$ ($\beta = \frac{1}{4}$). Our analysis was performed at a trial level, where the 18-second block were repeated ten times to compensate the filter's rise time requirement.

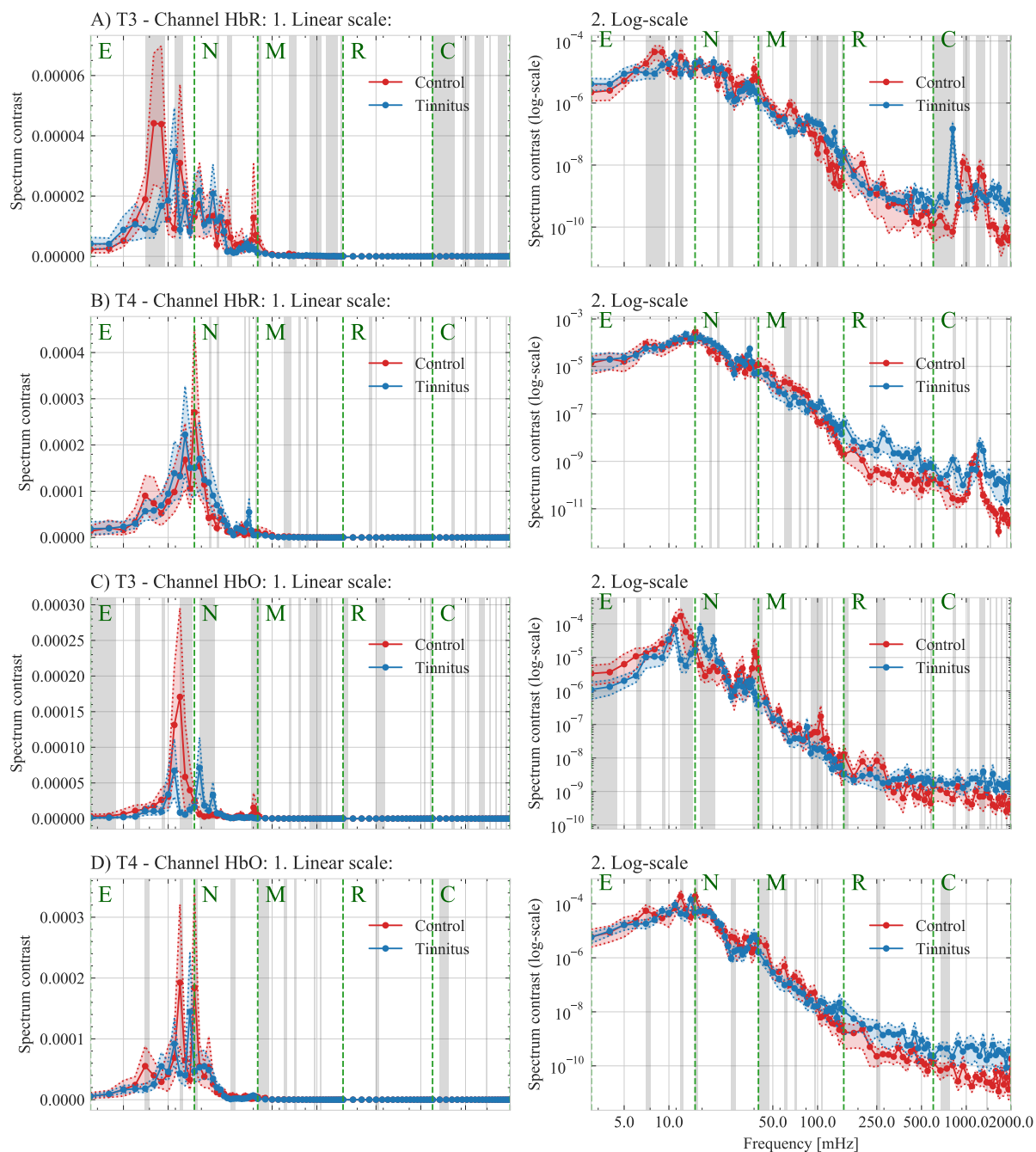


Figure 5: Sound spectrum contrast $c(\omega)$ for patients with tinnitus (PT) and the healthy control (HC) group in channels T3 and T4 for oxy- and deoxy-hemoglobin. Mean values are shown in bold lines, while dotted lines denote the 5th and 95th percentile of the estimates' distribution. Intervals of the ENMRC (endothelial, neurogenic, myogenic, respiratory and cardiac) scale are shown in dotted green lines. Black shadow regions denote the spectrum intervals with significant spectrum difference $d(\omega)$ between the PT and HC (p -value < 0.05).

Hb	Ch.	ENMRC scale	Frequency interval	Inter-group contrast		Significance (maxP method)	
				Mean, 95% C.I.	Min. t-value	Max. p-value	
HbR	T3	E	[7.000, 9.000)	1.599e-03; [1.073e-03, 2.106e-03]	3.032	2.694e-03 **	
		E	[11.000, 13.000)	-1.361e-05; [-1.436e-03, 1.445e-03]	-2.688	7.684e-03 **	
		N	[21.250, 22.500)	-7.732e-04; [-7.732e-04, -7.732e-04]	-2.422	1.619e-02 *	
		N	[25.000, 27.500)	6.203e-04; [4.564e-04, 7.831e-04]	2.395	1.736e-02 *	
		N	[35.000, 36.250)	3.759e-04; [3.759e-04, 3.759e-04]	2.380	1.811e-02 *	
		NM	[37.500, 45.000)	6.343e-04; [4.299e-04, 8.744e-04]	2.284	2.323e-02 *	
		M	[50.000, 55.000)	1.560e-04; [1.560e-04, 1.560e-04]	1.996	4.708e-02 *	
		M	[65.000, 75.000)	2.849e-04; [2.346e-04, 3.350e-04]	4.352	1.993e-05 ****	
		MR	[90.000, 150.000)	-1.147e-04; [-1.795e-04, -4.818e-05]	-2.891	4.185e-03 **	
		R	[250.000, 275.000)	-1.347e-05; [-1.347e-05, -1.347e-05]	-3.050	2.541e-03 **	
		R	[300.000, 350.000)	-9.696e-06; [-1.090e-05, -8.461e-06]	-2.833	4.996e-03 **	
		R	[375.000, 425.000)	-6.766e-06; [-8.224e-06, -5.294e-06]	-2.288	2.301e-02 *	
		RC	[450.000, 1090.000)	-1.233e-05; [-3.202e-05, 1.101e-06]	-2.165	3.136e-02 *	
		C	[1160.000, 1230.000)	-1.543e-05; [-1.543e-05, -1.543e-05]	-3.600	3.864e-04 ****	
		C	[1300.000, 1370.000)	1.226e-05; [1.226e-05, 1.226e-05]	2.248	2.550e-02 *	
		C	[1440.000, 2000.000)	-1.200e-05; [-1.511e-05, -9.196e-06]	-3.528	5.011e-04 ****	
	T4	E	[7.000, 8.000)	1.949e-03; [1.949e-03, 1.949e-03]	2.283	2.333e-02 *	
		EN	[15.000, 16.250)	3.279e-03; [3.279e-03, 3.279e-03]	2.164	3.141e-02 *	
		N	[18.750, 20.000)	-2.187e-03; [-2.187e-03, -2.187e-03]	-2.253	2.515e-02 *	
		N	[21.250, 22.500)	-2.397e-03; [-2.397e-03, -2.397e-03]	-3.278	1.198e-03 **	
		N	[32.500, 37.500)	-1.465e-03; [-2.209e-03, -7.654e-04]	-2.163	3.151e-02 *	
		NM	[38.750, 40.000)	7.618e-04; [7.618e-04, 7.618e-04]	2.609	9.652e-03 **	
		M	[60.000, 90.000)	2.963e-04; [1.662e-04, 4.326e-04]	2.564	1.096e-02 *	
		M	[100.000, 105.000)	-8.845e-05; [-8.845e-05, -8.845e-05]	-2.105	3.633e-02 *	
		M	[130.000, 135.000)	-4.033e-05; [-4.033e-05, -4.033e-05]	-2.045	4.199e-02 *	
		MR	[140.000, 350.000)	-2.747e-05; [-4.112e-05, -1.417e-05]	-2.106	3.624e-02 *	
		R	[375.000, 525.000)	-1.058e-05; [-1.302e-05, -7.467e-06]	-2.320	2.119e-02 *	
		R	[550.000, 575.000)	-5.152e-06; [-5.152e-06, -5.152e-06]	-2.149	3.263e-02 *	
C	[810.000, 1020.000)	-6.242e-06; [-1.242e-05, -2.233e-06]	-2.052	4.127e-02 *			
C	[1090.000, 1230.000)	8.663e-06; [4.478e-06, 1.289e-05]	2.176	3.052e-02 *			
C	[1300.000, 1720.000)	-5.317e-06; [-9.122e-06, -2.663e-06]	-2.272	2.396e-02 *			
C	[1790.000, 2000.000)	-2.784e-06; [-3.516e-06, -1.679e-06]	-2.432	1.574e-02 *			
HbO	T3	E	[3.000, 10.000)	8.066e-04; [1.148e-04, 1.503e-03]	2.289	2.295e-02 *	
		EN	[11.000, 15.000)	2.715e-03; [1.097e-03, 4.269e-03]	2.164	3.148e-02 *	
		N	[16.250, 21.250)	-1.551e-03; [-2.182e-03, -9.490e-04]	-2.379	1.816e-02 *	
		N	[26.250, 27.500)	2.396e-04; [2.396e-04, 2.396e-04]	2.407	1.686e-02 *	
		NM	[37.500, 45.000)	8.031e-04; [6.055e-04, 1.012e-03]	3.056	2.496e-03 **	
		M	[65.000, 70.000)	8.213e-05; [8.213e-05, 8.213e-05]	3.419	7.371e-04 ****	
		M	[90.000, 100.000)	4.988e-05; [3.977e-05, 5.995e-05]	2.545	1.154e-02 *	
		M	[105.000, 110.000)	1.130e-04; [1.130e-04, 1.130e-04]	3.472	6.128e-04 ****	
		M	[115.000, 120.000)	4.652e-05; [4.652e-05, 4.652e-05]	2.984	3.138e-03 **	
		MR	[150.000, 175.000)	2.245e-05; [2.245e-05, 2.245e-05]	2.579	1.051e-02 *	
		R	[375.000, 425.000)	-1.612e-05; [-2.373e-05, -8.605e-06]	-2.620	9.342e-03 **	
		R	[450.000, 500.000)	-1.236e-05; [-1.265e-05, -1.207e-05]	-2.600	9.897e-03 **	
		R	[525.000, 550.000)	-1.173e-05; [-1.173e-05, -1.173e-05]	-3.134	1.936e-03 **	
		RC	[575.000, 600.000)	-1.519e-05; [-1.519e-05, -1.519e-05]	-3.907	1.215e-04 ****	
		C	[670.000, 880.000)	-1.186e-05; [-1.429e-05, -9.391e-06]	-2.318	2.127e-02 *	
		C	[1020.000, 1370.000)	-1.449e-05; [-1.861e-05, -1.084e-05]	-2.269	2.412e-02 *	
	C	[1440.000, 2000.000)	-1.179e-05; [-1.393e-05, -9.765e-06]	-2.189	2.953e-02 *		
	T4	E	[7.000, 8.000)	1.719e-03; [1.719e-03, 1.719e-03]	2.836	4.953e-03 **	
		E	[12.000, 14.000)	2.553e-03; [1.100e-03, 4.021e-03]	2.354	1.938e-02 *	
		EN	[15.000, 16.250)	2.757e-03; [2.757e-03, 2.757e-03]	2.490	1.346e-02 *	
		N	[20.000, 21.250)	-1.119e-03; [-1.119e-03, -1.119e-03]	-1.996	4.708e-02 *	
		N	[26.250, 28.750)	4.849e-04; [4.363e-04, 5.318e-04]	2.162	3.163e-02 *	
		N	[31.250, 33.750)	4.020e-04; [1.104e-04, 6.965e-04]	2.165	3.134e-02 *	
		NM	[40.000, 50.000)	3.907e-04; [2.575e-04, 5.631e-04]	2.010	4.558e-02 *	
		M	[55.000, 65.000)	1.283e-04; [1.031e-04, 1.527e-04]	1.994	4.727e-02 *	
		M	[70.000, 75.000)	1.211e-04; [1.211e-04, 1.211e-04]	3.025	2.756e-03 **	
		M	[105.000, 110.000)	-3.801e-05; [-3.801e-05, -3.801e-05]	-2.529	1.209e-02 *	
		M	[125.000, 130.000)	-2.070e-05; [-2.070e-05, -2.070e-05]	-2.045	4.195e-02 *	
M		[140.000, 145.000)	-3.091e-05; [-3.091e-05, -3.091e-05]	-2.075	3.904e-02 *		
R	[225.000, 275.000)	-1.374e-05; [-1.645e-05, -1.103e-05]	-2.206	2.833e-02 *			
R	[325.000, 375.000)	-8.603e-06; [-9.458e-06, -7.747e-06]	-2.137	3.363e-02 *			
R	[400.000, 425.000)	-5.835e-06; [-5.835e-06, -5.835e-06]	-2.516	1.254e-02 *			
R	[500.000, 575.000)	-6.254e-06; [-8.632e-06, -4.621e-06]	-2.320	2.118e-02 *			
C	[670.000, 1300.000)	-5.237e-06; [-6.298e-06, -4.118e-06]	-1.989	4.780e-02 *			
C	[1370.000, 1580.000)	-5.035e-06; [-6.648e-06, -3.922e-06]	-2.515	1.256e-02 *			
C	[1650.000, 2000.000)	-4.832e-06; [-5.820e-06, -3.681e-06]	-2.192	2.934e-02 *			

Table 1: Frequency regions with statistically significant spectrum difference $d(\omega)$ between the tinnitus and control group. Uncertainty using p-values is also denoted: * ($P \leq 0.05$), ** ($P \leq 0.01$), *** ($P \leq 1e-3$), **** ($P \leq 1e-4$)

Frequency [mHz]	T3 (HbR)		T4 (HbR)		T3 (HbO)		T4 (HbO)	
	t-value	p-value	t-value	p-value	t-value	p-value	t-value	p-value
3.000	-0.847	3.976e-01	-0.081	9.356e-01	3.275	1.213e-03 **	-0.072	0.9426
4.000	-1.632	1.041e-01	0.550	5.827e-01	2.921	3.817e-03 **	-1.157	0.2484
5.000	-0.417	6.771e-01	-1.329	1.852e-01	2.289	2.295e-02 *	-0.739	0.4607
6.000	1.660	9.819e-02	-0.731	4.656e-01	2.904	4.023e-03 **	0.276	0.7824
7.000	3.032	2.694e-03 **	2.283	2.333e-02 *	2.429	1.587e-02 *	2.836	4.953e-03 **
8.000	4.274	2.763e-05 ****	0.874	3.829e-01	2.796	5.584e-03 **	1.716	0.08738
9.000	1.494	1.364e-01	-1.155	2.491e-01	3.373	8.653e-04 ****	-1.54	0.125
10.000	-0.632	5.280e-01	-1.093	2.755e-01	1.233	2.189e-01	-1.83	0.06848
11.000	-2.688	7.684e-03 **	-0.577	5.647e-01	2.387	1.777e-02 *	-0.676	0.4999
12.000	3.395	8.015e-04 ***	0.398	6.911e-01	5.136	5.796e-07 ****	3.201	1.553e-03 **
13.000	0.555	5.796e-01	-0.225	8.222e-01	3.465	6.268e-04 ****	2.354	1.938e-02 *
14.000	0.596	5.515e-01	-0.307	7.590e-01	2.164	3.148e-02 *	-1.925	0.05539
15.000	-0.642	5.214e-01	2.164	3.141e-02 *	0.900	3.691e-01	2.49	1.346e-02 *
15.000	-0.642	5.214e-01	2.164	3.141e-02 *	0.900	3.691e-01	2.49	1.346e-02 *
16.250	-1.951	5.221e-02	0.209	8.350e-01	-2.790	5.687e-03 **	-0.228	0.8202
17.500	-0.393	6.947e-01	0.190	8.492e-01	-3.616	3.648e-04 ***	-1.012	0.3125
18.750	0.040	9.678e-01	-2.253	2.515e-02 *	-2.379	1.816e-02 *	-1.095	0.2744
20.000	-1.042	2.985e-01	-1.422	1.563e-01	-3.159	1.786e-03 **	-1.996	4.708e-02 *
21.250	-2.422	1.619e-02 *	-3.278	1.198e-03 **	-1.656	9.904e-02	-1.824	0.06936
22.500	-0.260	7.953e-01	-1.131	2.590e-01	-0.516	6.061e-01	-1.636	0.1032
23.750	-0.967	3.347e-01	0.637	5.250e-01	-0.690	4.907e-01	0.522	0.6021
25.000	2.771	6.023e-03 **	-1.065	2.878e-01	0.662	5.087e-01	0.131	0.8958
26.250	2.395	1.736e-02 *	0.232	8.168e-01	2.407	1.686e-02 *	2.838	4.929e-03 **
27.500	-0.087	9.309e-01	1.547	1.231e-01	-1.129	2.600e-01	2.162	3.163e-02 *
28.750	1.295	1.964e-01	-1.687	9.284e-02	0.967	3.343e-01	0.975	0.3305
30.000	0.847	3.977e-01	-0.645	5.198e-01	1.597	1.116e-01	0.624	0.5331
31.250	0.472	6.373e-01	0.702	4.835e-01	1.423	1.561e-01	2.165	3.134e-02 *
32.500	1.262	2.083e-01	-2.874	4.410e-03 **	0.798	4.257e-01	2.586	1.031e-02 *
33.750	-0.096	9.238e-01	-2.714	7.124e-03 **	-0.533	5.948e-01	1.257	0.21
35.000	2.380	1.811e-02 *	-3.940	1.069e-04 ****	1.945	5.291e-02	-0.82	0.413
36.250	1.602	1.104e-01	-2.163	3.151e-02 *	1.502	1.343e-01	-1.882	0.06107
37.500	2.660	8.350e-03 **	0.096	9.238e-01	3.056	2.496e-03 **	-1.308	0.1922
38.750	2.284	2.323e-02 *	2.609	9.652e-03 **	3.848	1.528e-04 ****	1.027	0.3053
40.000	3.451	6.587e-04 ***	0.245	8.065e-01	4.002	8.354e-05 ****	2.01	4.558e-02 *

Table 2: Very-low-frequency spectrum differences $d(\omega)$ between the tinnitus and control group. Difference uncertainties in the endothelial (3-13mHz) and neurogenic (13-40mHz) bands are denoted with their significance. Uncertainty using p-values is also denoted: * ($P \leq 0.05$), ** ($P \leq 0.01$), *** ($P \leq 1e-3$), **** ($P \leq 1e-4$)

Moreover, we emphasize very-low-frequency intervals given the lack of tools to analyze them in finite-length samples properly. Let us consider the very-low-frequency oscillations in the spectral region of 3-20mHz, i.e., the endothelial or metabolic components in the ENMRC scale: a 5mHz-component requires 200 seconds (4000 time points) to complete a single cycle. Designing lengthy experiments that monitor the patient during several trials of this length will involve prolonged recording times that could represent an issue due to fatigue, exhaustion, discomfort, or pain during prolonged use of fNIRS devices [32]. Compared with the standard spectral analysis using FFT, COFRE can provide consistent estimators with limited amounts of data according to the precision required.

Using the limiting distribution of Equation 36, we can estimate the mean $d(\omega)$ and construct confidence intervals to the evaluated frequencies. Across the spectrum range, it was recognized that there is a substantial variation in the spectrum contrast between HC and PT (Figure 5). As an additional consequence of Equation 36, we can apply a Student's t-test two compare the PT and HC groups ([33, eq. 1], we then determine the frequency components where the contrast is statistically significant and ($p\text{-value} < 0.05$). We use the maximum p-value (maxP) procedure to combine consecutive significant harmonics ($p\text{-value} < 0.05$) into significant frequency regions [34, 35]. A comprehensive list of the most distinctive intervals along with their p-values is shown in Table 1. Also, note that t-values can be interpreted as unitless adjusted distances between the spectrum contrast $c(\omega|g)$ in the HC and PT groups.

Furthermore, several data-driven characteristics observed in this dataset can be distinguished. First, patients with tinnitus denote a spectral contrast $c(\omega|g)$ higher than the healthy control group in the respiratory and cardiac components, while they seem to have a lower contrast in

the 7-13mHz endothelial components, with a notorious impact in the channel T3 located in the left temporal lobe (Figure 5.C).

As expected, the magnitude of the contrasts $c(\omega|g)$ is inversely proportional to the frequency with a large part of the density concentrated in the low-frequency components. Therefore, to visually inspect the effects and variations between HC and PT in the entire range 3 – 2000mHz, we displayed the curves of $\mathbb{E}c(\omega|g)$ and $\log \mathbb{E}c(\omega|g)$ in Figure 5. Two local maxima are remarkable in those curves : (a.) in the region containing upper-metabolic and lower-neurogenic waves, and (b.) in the cardiac region.

In the first local-maxima neighborhood, the contrast in the left hemisphere is also always lower for tinnitus subjects in the ranges 3-10mHz ($|t\text{-value}| \geq 2.289$) and 11-15mHz ($|t\text{-value}| \geq 2.164$) in the endothelial region. Outside this pattern, no consistent difference $d(\omega)$ was found except in the harmonics at 7mHz ($|t\text{-value}| \geq 2.429$) and 12mHz ($|t\text{-value}| \geq 0.398$) where the contrast in subjects tinnitus is always lower than in the control group. These types of frequencies are believed to be caused by vasomotion regulation mechanisms [14, 36] or originated by metabolic processes in deeper layers of the brain [37]. However, further research should be performed to assess if the observed variation is solely related to the tinnitus condition and not from tinnitus' side effects or symptoms.

The second local maxima are observed in the cardiac region. Note that the contrast response of the tinnitus group in this entire interval is always higher than the control group in every analyzed condition: left and right hemisphere, and oxy- and deoxy-hemoglobin. We can understand from this metric that sound is correlated with a high variation of cardiovascular oscillations in the subjects with tinnitus compared to the healthy group. The dataset used in this study did not include an intraarterial subtraction angiography to evaluate subjective pulsatile tinnitus as Sila et al. recommended [38]. However, we can postulate that the observed variations in cardiac components could be biomarkers of pulsatile tinnitus in the current sample dataset.

Even though that distinctive spectrum patterns were found between PT and HC, no common pattern was found in the respiratory waves across chromophores and hemispheres. Nevertheless, we found that some neurogenic-myogenic signatures appear in the range of 37-50mHz with $|t\text{-values}|$ between 2.010 (HbO, T4) and 3.046 (HbO, T3).

5. Conclusion

This paper proposes a new method for spectrum estimation, the Complex-Pole Filter Representation (COFRE), to accurately discover discriminatory frequency signatures on fNIRS signals between patients with tinnitus and healthy control groups as a proof-of-concept. The spectral information contained in biomedical signals can be modeled using filter banks with narrow bandwidths. COFRE used this representation as a framework to propose a spectrum estimation based on narrow-band filters with a single complex pole (Equation 10).

COFRE inherits several relevant characteristics from the narrow-band filters that comprised it. COFRE filters can be configured to have the desired frequency resolution (Lemma 6) or maximum rise time as a transient time response metric (Lemma 8). As expected, in this setting, improving the time response could reduce the frequency response and vice versa. An upper-bound for this joint restriction was also formalized in Lemma 10. Furthermore, COFRE filters have a constant time and space complexity $\mathcal{O}(1)$ that support real-time applications or processing on memory-constrained systems.

We benefit from the properties of the COFRE spectrum representation to examine notable changes in the hemodynamic characteristics that could be related to a tinnitus condition. The interpretation was performed within the biological framework described by the ENMRC spectral division. Thus, we could observe specific oscillations that could serve as biomarkers: at 7mHz in the metabolic frequency region; and variations in the 30-50mHz in the neurogenic/myogenic band. Furthermore, notable, statistically significant, differences were denoted in the whole spectral bands related to respiratory and cardiac responses.

Even though this research was based on hemodynamic responses in tinnitus, we believe COFRE has the ability to be used in other studies involving biomedical signals where (a.) accurate estimation of exact frequency components is needed, (b.) spectral information is biologically interpretable, or (c.) time- or space-optimal algorithms for spectral estimation are expected.

Appendix A Narrow band-pass filter properties

A.1 Symmetric response

Lemma (Symmetry response). *A complex single-pole IIR filter defined by the transfer function $M(\omega; \rho, \omega^*)$ is symmetric around ω^* , i.e., $M(\omega; \rho, \omega^* - \Delta\omega) = M(\omega; \rho, \omega^* + \Delta\omega)$ $\Delta\omega \in [0, \frac{1}{2}]$.*

Proof. The magnitude response (Equation 13) can also be expressed as

$$M(z; \rho, \omega^*) = |H(\exp(j2\pi\omega))| = \left((1 - \rho \cos(2\pi(\omega^* - \omega)))^2 + \rho^2 \sin^2(2\pi(\omega^* - \omega)) \right)^{-\frac{1}{2}} \quad (37)$$

Now, let us examine the magnitude in the neighborhood of ω^* through $\omega = \omega^* + D$, $D > 0$:

$$|H(\exp(j2\pi(\omega^* + D)))| = \left((1 - \rho \cos(2\pi D))^2 + \rho^2 \sin^2(2\pi D) \right)^{-\frac{1}{2}} \quad (38)$$

Then, it is straightforward to corroborate that

$$|H(\exp(j2\pi(\omega^* - D)))| = \left((1 - \rho \cos(2\pi D))^2 + \rho^2 \sin^2(-2\pi D) \right)^{-\frac{1}{2}} = |H(\exp(j2\pi(\omega^* + D)))| \quad (39)$$

□

A.2 Unique maximum

Lemma (Unique maximum). *The filter $M(\omega; \rho, \Delta\omega)$ has a single and unique maximum located at ω^* and*

$$\max M(\omega; \rho, \omega) = M(\omega; \rho, \omega^*) = |1 - \rho|^{-1} \quad (40)$$

Proof. Let us examine the maximum filter magnitude (Equation 13),

$$\begin{aligned} \max M(\omega; \rho, \omega) &= \max |H(e^{j2\pi\omega})| = \max \frac{1}{|1 - \rho e^{j2\pi(\omega^* - \omega)}|} = \min |1 - \rho e^{j2\pi(\omega^* - \omega)}| \\ &= \min \sqrt{(1 - \rho \cos(2\pi(\omega^* - \omega)))^2 + \rho^2 \sin^2(2\pi(\omega^* - \omega))} \end{aligned} \quad (41)$$

Recall that $f(z) = \sqrt{z}$ is a concave function. Therefore, $\min \sqrt{z} = \sqrt{\min z}$ and

$$\max |H(e^{j2\pi\omega})| = \sqrt{\min f(\omega)} \quad (42)$$

where $f(\omega) = (1 - \rho \cos(2\pi\omega^* - 2\pi\omega))^2 + \rho^2 \sin^2(2\pi\omega^* - 2\pi\omega)$.

Note that the extrema in $f(\omega)$ are going to satisfy

$$\frac{d}{d\omega} f(\omega) = -2\rho \sin(2\pi(\omega^* - \omega)) = 0 \quad (43)$$

As a consequence of this expression, we have a periodic number of solutions (extreme values) at $\omega = \omega^* + \frac{1}{2}\ell$, $\ell = 0, 1, \dots$. However, in the frequency interval defined by the filter $H(e^{j\omega})$: $\omega \in [0, \frac{1}{2}]$, the only critical point is located at $\omega = \omega^*$.

To corroborate that the extreme at ω^* is a maximum, we can evaluate the second derivative of $f(\omega)$ at the point $\omega = \omega^*$:

$$g(\omega^*) = \frac{d^2}{d\omega^2} f(\omega) \Big|_{\omega=\omega^*} = 2\rho \cos(2\pi\omega^* - 2\pi\omega) = 2\rho > 0 \quad (44)$$

Then, $g(\omega^*)$ is always positive for any $0 < \rho \leq 1$, and $\omega = \omega^*$ is the unique maximum in $[0, \pi]$. □

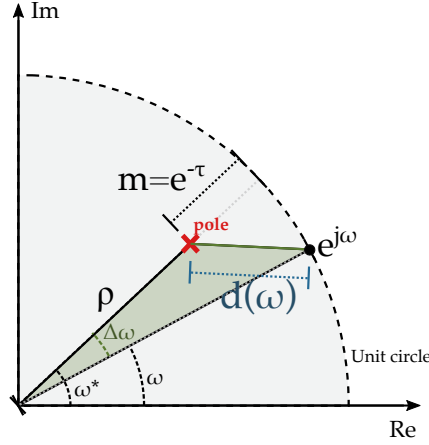


Figure 6: Geometric interpretation of the complex pole of a filter $M(\omega; \rho, \omega^*)$

A.3 Frequency resolution

Lemma (Frequency resolution configuration). *The cosine of the frequency resolution of a filter $M(\omega; \rho, \omega^*)$ is a second-order rational function of the complex autoregressive modulus ρ :*

$$\Delta\omega = \frac{1}{2\pi} \arccos\left(\frac{1}{2\rho} (\rho^2 + 1 - \alpha^{-2} (1 - \rho)^2)\right) \quad (45)$$

Proof. Recall the magnitude response (Equation 13) at a frequency ω :

$$\left|H(e^{j\omega})\right| = \frac{1}{|1 - \rho e^{j2\pi(\omega^* - \omega)}|} = \frac{|e^{j2\pi\omega}|}{|e^{j2\pi\omega} - \rho e^{j2\pi\omega^*}|} = \frac{1}{d(\omega)} \quad (46)$$

where $d(\omega) = |e^{j2\pi\omega} - \rho e^{j2\pi\omega^*}|$.

Note that $d(\omega)$ can be interpreted as the distance between the complex poles at ω and ω^* . In consequence, $d(\omega^*) = |1 - \rho|$. A graphical representation of $d(\omega)$ is depicted in Figure 6.

Let $\omega = \omega^* + \Delta\omega$, where $\Delta\omega$ is the frequency resolution (Corollary 4), then

$$d(\omega) = \frac{1}{M(\omega; \rho, \omega^* + \Delta\omega)} = \frac{1}{\alpha M(\omega; \rho, \omega^*)} = \frac{1}{\alpha} d(\omega^*) = \frac{1}{\alpha} |1 - \rho| \quad (47)$$

From the geometrical interpretation (Figure 6), it is straightforward to infer that $\Delta\omega$ and ρ are related through the law of cosines:

$$2\rho \cos 2\pi\Delta\omega = \rho^2 + 1 - d^2(\omega) = \rho^2 + 1 - \alpha^{-2} (1 - \rho)^2 \quad (48)$$

□

A.4 Frequency resolution

Corollary (Frequency-optimal bandwidth). *The minimum bandwidth τ to ensure a frequency resolution $\Delta\omega$ under a cut-off α is given by*

$$\tau = -\log\left(1 - \frac{\cos 2\pi\Delta\omega - \alpha^{-2}}{1 - \alpha^{-2}} - \frac{1}{1 - \alpha^{-2}} \sqrt{\cos^2 2\pi\Delta\omega - (1 - \alpha^{-2})^2}\right) \quad (49)$$

Proof. From the relationship between $\Delta\omega$ and ρ denoted in Equation 48, we obtain

$$0 = \rho^2 (1 - \alpha^{-2}) + 2\rho (\alpha^{-2} - \cos 2\pi\Delta\omega) + (1 - \alpha^{-2}) \quad (50)$$

Therefore,

$$\rho = \frac{\cos 2\pi\Delta\omega - \alpha^{-2}}{1 - \alpha^{-2}} \pm \frac{1}{1 - \alpha^{-2}} \sqrt{\cos^2 2\pi\Delta\omega - (1 - \alpha^{-2})^2} \quad (51)$$

Note that given that $\rho \geq 0$, the negative root of the quadratic expression will be ignored.

Finally, recall the equivalency between the bandwidth τ and the modulus ρ : $\rho = 1 - e^{-\tau}$. Then,

$$e^{-\tau} = 1 - \frac{\cos 2\pi\Delta\omega - \alpha^{-2}}{1 - \alpha^{-2}} - \frac{1}{1 - \alpha^{-2}} \sqrt{\cos^2 2\pi\Delta\omega - (1 - \alpha^{-2})^2} \quad (52)$$

□

A.5 Rise time

Lemma (Rise time configuration). *The rise time of a filter $M(\omega; \rho, \omega^*)$ is inversely proportional to the logarithm of ρ and proportional to the logarithm of the complement of the cut-off factor β :*

$$t^* = \log_{\rho} \left(\frac{1 - \beta}{\rho} \right) = \frac{\log(1 - \beta)}{\log(\rho)} - 1 \quad (53)$$

Proof. Recall the transfer function of the filter (Equation 12):

$$H(z) = \frac{1}{1 - \rho e^{j2\pi\omega^*} z^{-1}} = F(z; \rho, \omega^*) \quad (54)$$

Without loss of generality, we can assume a complex input signal $x(t) = \exp(j2\pi vt)$, where $v \in [0, \frac{1}{2}]$. Then, the output of the filter is

$$Y(z) = \frac{1}{1 - \rho e^{j2\pi\omega^*} z^{-1}} \frac{1}{1 - e^{j2\pi v} z^{-1}} \quad (55)$$

Solving by partial fractions, we obtain

$$Y(z) = \frac{1}{e^{j2\pi v} - \rho e^{j2\pi\omega^*}} \left(\frac{e^{j2\pi v}}{1 - e^{j2\pi v} z^{-1}} - \frac{\rho e^{j2\pi\omega^*}}{1 - \rho e^{j2\pi\omega^*} z^{-1}} \right) \quad (56)$$

Therefore, the inverse z-transform of $Y(z)$: $y(t)$ is given by

$$y(t) = \frac{1}{e^{j2\pi v} - \rho e^{j2\pi\omega^*}} \left(e^{j2\pi v} e^{j2\pi vt} - \rho^{t+1} e^{j2\pi\omega^*} e^{j2\pi\omega^* t} \right) \quad (57)$$

Now, let us assume that the input signal is resonating at the central frequency of the filter ($v = \omega^*$):

$$y(t) = \frac{1 - \rho^{t+1}}{1 - \rho} e^{j2\pi\omega^* t} \quad (58)$$

Then, the real component of $y(t)$ is defined as

$$y^*(t) = \text{Re}(y(t)) = \frac{1 - \rho^{t+1}}{1 - \rho} \cos(2\pi\omega^* t) = A(t) \cos(2\pi\omega^* t) \quad (59)$$

We can denote that the envelope $A(t)$ is determining the transient behavior of the filter. In a stable filter ($\rho < 1$), the envelope converges to A_{\max} at the infinite:

$$\lim_{t \rightarrow \infty} \left(\frac{1 - \rho^{t+1}}{1 - \rho} \right) = \frac{1}{1 - \rho} = A_{\max} \quad (60)$$

Consequently, the time t^* needed to for $A(t)$ to “rise” from 0 to βA_{\max} (Definition 5) satisfies

$$\beta \frac{1}{1 - \rho} = \frac{1 - \rho^{t^*+1}}{1 - \rho} \quad (61)$$

Therefore, t^* , when $0 < \rho < 1$, is determined by

$$t^* = \frac{\log(1 - \beta)}{\log(\rho)} - 1 = \log_{\rho} \left(\frac{1 - \beta}{\rho} \right) \quad (62)$$

□

A.6 Time-optimal bandwidth

Corollary (Time-optimal bandwidth). *The minimum bandwidth τ to ensure a rise time t^* (under a cut-off β) is*

$$\tau = -\log \left(1 - (1 - \beta)^{\frac{1}{1+t^*}} \right) \quad (63)$$

Proof. Recall Equation 62, and rearrange it:

$$\log(\rho) = \frac{\log(1 - \beta)}{1 + t^*} \quad (64)$$

Then, we can describe ρ as a function of the cut-off and rise-time t^* :

$$\rho = (1 - \beta)^{\frac{1}{1+t^*}} \quad (65)$$

Now, given the bandwidth-modulus relationship $\rho = 1 - e^{-\tau}$,

$$e^{-\tau} = 1 - (1 - \beta)^{\frac{1}{1+t^*}} \quad (66)$$

□

A.7 Time-frequency constraint

Lemma (Joint time-frequency constraint). *Given the cut-offs α and β , the rise time t^* and the frequency resolution $\Delta\omega$ are mutually constrained by*

$$t^* \Delta\omega < -\log(1 - \beta) \left(\frac{\sqrt{(\alpha\pi\Delta\omega)^2 - \alpha^2 + 1}}{2\pi\alpha} + \frac{\Delta\omega}{2} \right) - \Delta\omega \quad (67)$$

Proof. Let us analyze the Maclaurin series of the cosine function:

$$\cos z = \sum_{k=0}^{\infty} \frac{1}{(2k)!} (-1)^k z^{2k} = 1 - \frac{1}{2!} z^2 + \frac{1}{4!} z^4 - \frac{1}{6!} z^6 + \dots \quad (68)$$

The radius of convergence $r_{k \rightarrow k+1}^{(c)}$ of this series is given by

$$r_{k \rightarrow k+1}^{(c)} = \frac{\frac{1}{(2k+2)!} (-1)^{k+1} z^{2(k+1)}}{\frac{1}{(2k)!} (-1)^k z^{2k}} = -\frac{z^2}{(2k+2)(2k+1)} \quad (69)$$

It is remarkable that $|r_{k \rightarrow k+1}^{(c)}| < 1$, and consequently,

$$\left(1 - |r_{k \rightarrow k+1}^{(c)}| \left(1 - |r_{k+1 \rightarrow k+2}^{(c)}| (1 - \dots)\right)\right) < 1 \quad (70)$$

Now, let us examine the series expansion of the logarithm function,

$$\log(1-z) = -\sum_{k=1}^{\infty} \frac{1}{k} z^k = -z - \frac{1}{2}z^2 - \frac{1}{3}z^3 - \frac{1}{4}z^4 + \dots \quad (71)$$

with its inherent radius of convergence,

$$r_{k \rightarrow k+1}^{(l)} = \frac{\frac{-1}{(k+1)} z^{(k+1)}}{\frac{-1}{k} z^k} = \frac{1}{1 + \frac{1}{k}} z \quad (72)$$

It is clear that the convergence of the series is ensured when $z < 1$, satisfying also the following inequality:

$$\left(1 + r_{k \rightarrow k+1}^{(l)} \left(1 + r_{k+1 \rightarrow k+2}^{(l)} (1 + \dots)\right)\right) > 1 \quad (73)$$

Provided the previous inequalities, we can establish some boundaries for $\cos z$ and $\log(1+z)$:

$$\cos z = 1 - \frac{z^2}{2} \left(1 - \frac{z^2}{12} \left(1 - \frac{z^2}{40} (1 - \dots)\right)\right) > 1 - \frac{z^2}{2} \quad (74)$$

$$\log(1+z) = -z \left(1 + \frac{z}{2} \left(1 + \frac{z}{1 + \frac{1}{2}} (1 - \dots)\right)\right) < -z \quad 0 < z < 1 \quad (75)$$

Now, recall [Equation 48](#),

$$\cos 2\pi\Delta\omega = \frac{1}{2\rho} \left(1 + \rho^2 - \alpha^{-2} (1 - \rho)^2\right) \quad (76)$$

By applying the upperbound of [Equation 74](#), we obtain

$$1 - \frac{1}{2} (2\pi\Delta\omega)^2 > \frac{1}{2\rho} \left(1 + \rho^2 - \alpha^{-2} (1 - \rho)^2\right) \quad (77)$$

For brevity in the notation, let $v = 2\pi\Delta\omega$ and $u = (1 - \rho)$:

$$\begin{aligned} v^2 &< 2 - \frac{1}{\rho} \left(1 + \rho^2 - \alpha^{-2} u^2\right) \\ &< -\frac{1}{\rho} \left(1 - 2\rho + \rho^2 - \alpha^{-2} u^2\right) \\ &< -\frac{1}{1-u} \left(u^2 - \alpha^{-2} u^2\right) \end{aligned} \quad (78)$$

Furthermore, let $a = (1 - \alpha^{-2})$, then

$$w^2 < -a \frac{u^2}{1-u} \quad (79)$$

$$au^2 - w^2u + w^2 < 0 \quad (80)$$

Later, recall [Equation 62](#),

$$\log(1 - (1 - \rho)) = \frac{1}{(1 + t^*)} \log(1 - \beta) \quad (81)$$

Let $b = \log(1 - \beta)$ and $T = (1 + t^*)$, and use the boundary in [Equation 75](#),

$$\begin{aligned} -u &< \frac{1}{(1 + t^*)} \log(1 - \beta) = \frac{b}{T} \\ u &> -\frac{b}{T} \end{aligned} \quad (82)$$

Note that $u \in (0, 1)$ and $a < 0$, then

$$-wu < w \frac{b}{T} \quad (83)$$

$$au^2 < a \frac{b^2}{T^2} \quad (84)$$

Replacing both expressions in [Equation 80](#),

$$a \frac{b^2}{T^2} - w \frac{b}{T} + w^2 < 0 \quad (85)$$

Therefore,

$$(Tw)^2 + b(Tw)w + ab^2 < 0 \quad (86)$$

Factorizing the left side of the inequality,

$$\left(Tw - \frac{1}{2}b(\sqrt{w^2 - 4a} + w)\right) \left(Tw - \frac{1}{2}b(-\sqrt{w^2 - 4a} + w)\right) < 0 \quad (87)$$

$$Tw < \frac{1}{2}b(\sqrt{w^2 - 4a} + w) \quad (88)$$

Now, reformulating the inequality in terms of $\Delta\omega$ and t^* ,

$$t^*\Delta\omega < -\log(1 - \beta) \left(\frac{\sqrt{(\alpha\pi\Delta\omega)^2 - \alpha^2 + 1}}{2\pi\alpha} + \frac{\Delta\omega}{2} \right) - \Delta\omega \quad (89)$$

Note that $(\alpha\pi\Delta\omega)^2 - \alpha^2 + 1 > 0 \quad \forall \Delta\omega \in [0, \frac{1}{2}]$.

Let us consider bandpass filters with frequency resolution $\Delta\omega < \frac{1}{5}$, then the time-frequency constraint can be upper-bounded by

$$t^*\Delta\omega < -\log(1 - \beta) \left(\frac{\sqrt{1 - (1 + \frac{4}{25}\pi^2)\alpha^2}}{2\pi\alpha} + \frac{1}{10} \right) - \frac{1}{5} \quad (90)$$

Furthermore, in filters with extremely low frequency resolution $\Delta\omega \rightarrow 0$, [Equation 89](#) can be simplified to

$$t^*\Delta\omega < -\log(1 - \beta) \left(\frac{\sqrt{1 - \alpha^2}}{2\pi\alpha} \right) \quad (91)$$

□

References

- [1] A. R. Møller, B. Langguth, D. De Ridder, T. Kleinjung (Eds.), *Textbook of Tinnitus*, Springer New York, New York, NY, 2011. doi:10.1007/978-1-60761-145-5.
- [2] R. S. Tyler (Ed.), *Tinnitus Treatment: Clinical Protocols*, Thieme, New York, 2006.
- [3] P. J. Jastreboff, W. C. Gray, S. L. Gold, Neurophysiological approach to tinnitus patients, *The American Journal of Otology* 17 (2) (1996) 236–240.
- [4] P. J. Jastreboff, Phantom auditory perception (tinnitus): Mechanisms of generation and perception, *Neuroscience Research* 8 (4) (1990) 221–254. doi:10.1016/0168-0102(90)90031-9.
- [5] D. Baguley (Ed.), *Tinnitus: A Multidisciplinary Approach*, 2nd Edition, Wiley-Blackwell, Chichester, West Sussex, UK ; Hoboken, NJ, USA, 2013.
- [6] J. J. Eggermont, *The Neuroscience of Tinnitus*, Oxford University Press, Oxford, United Kingdom, 2012.
- [7] A. B. G. Sevy, H. Bortfeld, T. J. Huppert, M. S. Beauchamp, R. E. Tonini, J. S. Oghalai, Neuroimaging with near-infrared spectroscopy demonstrates speech-evoked activity in the auditory cortex of deaf children following cochlear implantation, *Hearing Research* 270 (1-2) (2010) 39–47. doi:10.1016/j.heares.2010.09.010.
- [8] C. Olds, L. Pollonini, H. Abaya, J. Larky, M. Loy, H. Bortfeld, M. S. Beauchamp, J. S. Oghalai, Cortical Activation Patterns Correlate with Speech Understanding After Cochlear Implantation, *Ear & Hearing* 37 (3) (2016) e160–e172. doi:10.1097/AUD.000000000000258.
- [9] M. Schecklmann, A. Giani, S. Tupak, B. Langguth, V. Raab, T. Polak, C. Várallyay, W. Harnisch, M. J. Herrmann, A. J. Fallgatter, Functional Near-Infrared Spectroscopy to Probe State- and Trait-Like Conditions in Chronic Tinnitus: A Proof-of-Principle Study, *Neural Plasticity* 2014 (2014) 1–8. doi:10.1155/2014/894203.
- [10] M. Issa, S. Bisconti, I. Kovelman, P. Kileny, G. J. Basura, Human Auditory and Adjacent Nonauditory Cerebral Cortices Are Hypermetabolic in Tinnitus as Measured by Functional Near-Infrared Spectroscopy (fNIRS), *Neural Plasticity* 2016 (2016) 1–13. doi:10.1155/2016/7453149.
- [11] A. Stefanovska, M. Bracic, H. Kvernmo, Wavelet analysis of oscillations in the peripheral blood circulation measured by laser Doppler technique, *IEEE Transactions on Biomedical Engineering* 46 (10) (Oct./1999) 1230–1239. doi:10.1109/10.790500.
- [12] M. J. Geyer, Y.-K. Jan, D. M. Brienza, M. L. Boninger, Using wavelet analysis to characterize the thermoregulatory mechanisms of sacral skin blood flow, *The Journal of Rehabilitation Research and Development* 41 (6) (2004) 797. doi:10.1682/JRRD.2003.10.0159.
- [13] A. Stefanovska, Physics of the human cardiovascular system, *Contemporary Physics* 40 (1) (1999) 31–55. doi:10.1080/001075199181693.
- [14] J. Kastrop, J. Bülow, N. A. Lassen, Vasomotion in human skin before and after local heating recorded with laser Doppler flowmetry. A method for induction of vasomotion, *International Journal of Microcirculation, Clinical and Experimental* 8 (2) (1989) 205–215.
- [15] T. Söderström, A. Stefanovska, M. Veber, H. Svensson, Involvement of sympathetic nerve activity in skin blood flow oscillations in humans, *American Journal of Physiology-Heart and Circulatory Physiology* 284 (5) (2003) H1638–H1646. doi:10.1152/ajpheart.00826.2000.
- [16] A. A. Mendelson, A. Rajaram, D. Bainbridge, K. S. Lawrence, T. Bentall, M. Sharpe, M. Diop, C. G. Ellis, Dynamic tracking of microvascular hemoglobin content for continuous perfusion monitoring in the intensive care unit: Pilot feasibility study, *Journal of Clinical Monitoring and Computing* (Oct. 2020). doi:10.1007/s10877-020-00611-x.
- [17] E. L. Urquhart, X. Wang, H. Liu, P. J. Fadel, G. Alexandrakis, Differences in Net Information Flow and Dynamic Connectivity Metrics Between Physically Active and Inactive Subjects Measured by Functional Near-Infrared Spectroscopy (fNIRS) During a Fatiguing Handgrip Task, *Frontiers in Neuroscience* 14 (2020) 167. doi:10.3389/fnins.2020.00167.
- [18] P. Pinti, D. Cardone, A. Merla, Simultaneous fNIRS and thermal infrared imaging during cognitive task reveal autonomic correlates of prefrontal cortex activity, *Scientific Reports* 5 (1) (2015) 17471. doi:10.1038/srep17471.
- [19] B. M. Bosch, A. Bringard, G. Ferretti, S. Schwartz, K. Iglói, Effect of cerebral vasomotion during physical exercise on associative memory, a near-infrared spectroscopy study, *Neurophotonics* 4 (4) (2017) 041404. doi:10.1117/1.nph.4.4.041404.
- [20] Z. Zhang, R. Khatami, Predominant endothelial vasomotor activity during human sleep: A near-infrared spectroscopy study, *European Journal of Neuroscience* 40 (9) (2014) 3396–3404. doi:10.1111/ejn.12702.

- [21] M. H. Hayes, *Statistical Digital Signal Processing and Modeling*, John Wiley and Sons, New York, 1996.
- [22] M. S. Folgosi, G. E. C. Nogueira, Quantifying low-frequency fluctuations in the laser Doppler flow signal from human skin, in: *SPIE BiOS*, San Francisco, California, USA, 2011, p. 789811. doi:10.1117/12.874080.
- [23] T. Q. D. Khoa, M. Nakagawa, Recognizing brain activities by functional near-infrared spectroscopy signal analysis, *Nonlinear Biomedical Physics* 2 (1) (2008) 3. doi:10.1186/1753-4631-2-3.
- [24] M. A. Arbib (Ed.), *The Handbook of Brain Theory and Neural Networks*, 2nd Edition, MIT Press, Cambridge, Mass, 2003.
- [25] F. A. Fishburn, R. S. Ludlum, C. J. Vaidya, A. V. Medvedev, Temporal Derivative Distribution Repair (TDDR): A motion correction method for fNIRS, *NeuroImage* 184 (2019) 171–179. doi:10.1016/j.neuroimage.2018.09.025.
- [26] T.-H. Li, *Time Series with Mixed Spectra*, CRC Press/Chapman & Hall, Boca Raton, Fla., 2014.
- [27] J. San Juan, X.-S. Hu, M. Issa, S. Bisconti, I. Kovelman, P. Kileny, G. Basura, Tinnitus alters resting state functional connectivity (RSFC) in human auditory and non-auditory brain regions as measured by functional near-infrared spectroscopy (fNIRS), *PLOS ONE* 12 (6) (2017) e0179150. doi:10.1371/journal.pone.0179150.
- [28] T. Jue, K. Masuda (Eds.), *Application of Near Infrared Spectroscopy in Biomedicine*, Springer US, 2013. doi:10.1007/978-1-4614-6252-1.
- [29] J. M. Schmitt, *Optical measurement of blood oxygenation by implantable telemetry*, Tech. rep., Stanford University (1986).
URL <https://books.google.no/books?id=jIgPIQAACAAJ>
- [30] M. K. Moaveni, *A Multiple Scattering Field Theory Applied to Whole Blood*, PhD Thesis, Department of Electrical Engineering, University of Washington (1970).
- [31] A. Duncan, J. H. Meek, M. Clemence, C. E. Elwell, P. Fallon, L. Tyszczuk, M. Cope, D. T. Delpy, Measurement of Cranial Optical Path Length as a Function of Age Using Phase Resolved Near Infrared Spectroscopy, *Pediatric Research* 39 (5) (1996) 889–894. doi:10.1203/00006450-199605000-00025.
- [32] A. Kassab, J. L. Lan, P. Vannasing, M. Sawan, Functional near-infrared spectroscopy caps for brain activity monitoring: A review, *Applied Optics* 54 (3) (2015) 576. doi:10.1364/AO.54.000576.
- [33] T. Lumley, P. Diehr, S. Emerson, L. Chen, The Importance of the Normality Assumption in Large Public Health Data Sets, *Annual Review of Public Health* 23 (1) (2002) 151–169. doi:10.1146/annurev.publhealth.23.100901.140546.
- [34] C. Song, G. C. Tseng, Hypothesis setting and order statistic for robust genomic meta-analysis, *The Annals of Applied Statistics* 8 (2) (2014) 777–800. doi:10.1214/13-aos683.
- [35] B. Wilkinson, A statistical consideration in psychological research, *Psychological Bulletin* 48 (3) (1951) 156–158. doi:10.1037/h0059111.
- [36] C. Aalkjaer, D. Boedtker, V. Matchkov, Vasomotion - what is currently thought?, *Acta Physiologica* 202 (3) (2011) 253–269. doi:10.1111/j.1748-1716.2011.02320.x.
- [37] H. Obrig, M. Neufang, R. Wenzel, M. Kohl, J. Steinbrink, K. Einhüpl, A. Villringer, Spontaneous Low Frequency Oscillations of Cerebral Hemodynamics and Metabolism in Human Adults, *NeuroImage* 12 (6) (2000) 623–639. doi:10.1006/nimg.2000.0657.
- [38] C. A. Sila, A. J. Furlan, J. R. Little, Pulsatile tinnitus., *Stroke* 18 (1) (1987) 252–256. doi:10.1161/01.STR.18.1.252.